

Development of a deep-water carbonate ion concentration proxy based on preservation of planktonic foraminifera shells quantified by X-ray CT scanning

Shinya Iwasaki¹, Katsunori Kimoto², and Michal Kucera³

¹MARUM - Center for Marine Environmental Sciences, University of Bremen

²Research Institute for Global Change, Japan Agency for Marine-Earth

³Marum Bremen

December 16, 2022

Abstract

The quantitative and objective characterization of dissolution intensity in fossil planktonic foraminiferal shells could be used to reconstruct past changes in bottom water carbonate ion concentration. Among proxies measuring the degree of dissolution of planktonic foraminiferal shells, X-ray micro-Computed Tomography (CT) based characterization of apparent shell density appears to have good potential to facilitate quantitative reconstruction of carbonate chemistry. However, unlike the well-established benthic foraminiferal B/Ca ratio-based proxy, only a regional calibration of the CT-based proxy exists based on a limited number of data points covering mainly low-saturation state waters. Here we determined by CT-based proxy the shell dissolution intensity of planktonic foraminifera Globigerina bulloides, Globorotalia inflata, Globigerinoides ruber, and Trilobatus sacculifer from a collection of core top samples in the Southern Atlantic covering higher saturation states, and assessed the characteristics and reliability of CT-based proxy. We observed that the CT-based proxy is generally controlled by deep-water $\Delta[\text{O}32^-]$ λικε της $\text{B}/\delta \text{ προξψ}$, βυτ ιτς εφφεστιε ρανγε οφ $\Delta[\text{O}32^-]$ ις βετωεεν -20 ιο 10 $\mu\text{mol kg}^{-1}$. In this range, the CT-based proxy appears directly and strongly related to deep-water $\Delta[\text{O}32^-]$, αηερεας της B/δ οφ βεντηις φοραμινιφερα αππεαρς το βε αφφεστεδ βψ πορεωατερ σατυρατιον ιν καρβονατε-ρικη συβστρατες. Ον τηε οτηερ ηανδ, τηε $^{\circ}\text{T}$ -βασεδ προξψ ις αφφεστεδ βψ συπραλψοσζλιναλ δισσολυτιον ιν αρεας αιτη ηιγη προδυςτιτψ. Λικε τηε B/δ προξψ, τηε $^{\circ}\text{T}$ -βασεδ προξψ ρεχυιρες σπεζιεσ-σπεζιψ καλιβρατιον, βυτ τηε εφφεστ οφ σπεζιεσ-σπεζιψ σηελλ διφφερενζε ιν συσζεπτιβιλιτψ το δισσολυτιον ον τηε προξψ ις σμαλλ.

Hosted file

952089_0_art_file_10538251_rmxcpk.docx available at <https://authorea.com/users/566861/articles/613443-development-of-a-deep-water-carbonate-ion-concentration-proxy-based-on-preservation-of-planktonic-foraminifera-shells-quantified-by-x-ray-ct-scanning>

1
2 **Development of a deep-water carbonate ion concentration proxy based on**
3 **preservation of planktonic foraminifera shells quantified by X-ray CT**
4 **scanning**

5
6 **S. Iwasaki^{1*}, K. Kimoto², M. Kucera¹**

7
8 ¹MARUM - Center for Marine Environmental Sciences, University of Bremen, Bremen,
9 Germany
10 ² Japan Agency for Marine-Earth Science and Technology, Research Institute for Global Change,
11 Yokosuka, Japan

12
13
14 Corresponding author: Shinya Iwasaki (siwasaki@marum.de)

15
16
17 **Key Points:**

- 18 • Planktonic foraminiferal shell dissolution intensity was determined by CT-based proxy
19 using core top samples in the Southern Atlantic Ocean.
- 20 • The characteristics and reliability of CT-based proxy were assessed by comparing with
21 conventional proxy.
- 22 • The CT-based proxy is available for reconstructing deep seawater carbonate ion
23 concentration under the appropriate condition.

26 **Abstract**

27 The quantitative and objective characterization of dissolution intensity in fossil planktonic
 28 foraminiferal shells could be used to reconstruct past changes in bottom water carbonate ion
 29 concentration. Among proxies measuring the degree of dissolution of planktonic foraminiferal
 30 shells, X-ray micro-Computed Tomography (CT) based characterization of apparent shell
 31 density appears to have good potential to facilitate quantitative reconstruction of carbonate
 32 chemistry. However, unlike the well-established benthic foraminiferal B/Ca ratio-based proxy,
 33 only a regional calibration of the CT-based proxy exists based on a limited number of data points
 34 covering mainly low-saturation state waters. Here we determined by CT-based proxy the shell
 35 dissolution intensity of planktonic foraminifera *Globigerina bulloides*, *Globorotalia inflata*,
 36 *Globigerinoides ruber*, and *Trilobatus sacculifer* from a collection of core top samples in the
 37 Southern Atlantic covering higher saturation states, and assessed the characteristics and
 38 reliability of CT-based proxy. We observed that the CT-based proxy is generally controlled by
 39 deep-water $\Delta[\text{CO}_3^{2-}]$ like the B/Ca proxy, but its effective range of $\Delta[\text{CO}_3^{2-}]$ is between -20 to
 40 $10 \mu\text{mol kg}^{-1}$. In this range, the CT-based proxy appears directly and strongly related to deep-
 41 water $\Delta[\text{CO}_3^{2-}]$, whereas the B/Ca of benthic foraminifera appears to be affected by porewater
 42 saturation in carbonate-rich substrates. On the other hand, the CT-based proxy is affected by
 43 supralysocinal dissolution in areas with high productivity. Like the B/Ca proxy, the CT-based
 44 proxy requires species-specific calibration, but the effect of species-specific shell difference in
 45 susceptibility to dissolution on the proxy is small.

46

47 **1 Introduction**

48 The atmospheric CO₂ concentration has fluctuated by ~80 ppm between glacial and
 49 interglacial periods, implying a large and rapid exchange of carbon between the atmosphere and
 50 the ocean on those time scales [Barnola et al., 1987; Petit et al., 1999]. This is because the
 51 oceanic carbon pool is about 50 times larger than that of the atmosphere [Sigman and Boyle,
 52 2000], and carbon storage in the deep ocean and changes in deep-water circulation can
 53 substantially alter atmospheric pCO₂. However, data concerning the amount of carbon storage in
 54 the deep sea and their temporal and spatial variation, which are essential to understand the
 55 glacial-interglacial pCO₂ exchange between ocean and atmosphere, is insufficient. Because the
 56 deep seawater carbonate ion concentration ($[\text{CO}_3^{2-}]$) is governed primarily by the concentration
 57 of dissolved inorganic carbon and alkalinity, its reconstruction can provide valuable insights into
 58 the changes in the global carbon cycle.

59 The B/Ca ratio of epifaunal benthic foraminifera has been proposed as a quantitative
 60 deep seawater $[\text{CO}_3^{2-}]$ proxy [e.g., Yu and Elderfield, 2007]. This proxy relies on the fact that
 61 the ratio of the two major boron species in the deep seawater, B(OH)₃ and B(OH)₄⁻, varies with
 62 pH [Hemming et al., 1992] and these variations are reflected in the B/Ca ratio in shell calcite.
 63 Indeed, a significant correlation between B/Ca ratio in the shells of *Cibicidoides wuellerstorfi*
 64 and deep seawater $\Delta[\text{CO}_3^{2-}]$ was shown by Yu and Elderfield [2007]. The sensitivity of *C.*
 65 *wuellerstorfi* B/Ca ratio to deep seawater $\Delta[\text{CO}_3^{2-}]$ was evaluated based on core-top calibration
 66 at more than 200 sites, indicating an uncertainty of $\pm 5 \mu\text{mol kg}^{-1}$ in $[\text{CO}_3^{2-}]$ (Brown and
 67 Elderfield, 1996, Rae et al., 2011, Raitzsch et al., 2011, Yu and Elderfield., 2007, Yu et al., 2013,
 68 2014, Brown et al., 2011). Based on this calibration, subsequent studies reconstructed temporal
 69 variations in deep seawater $[\text{CO}_3^{2-}]$ at several sites, where the sediment samples contain

70 sufficient amount of benthic foraminifera shells of the target species [e.g., [Yu et al., 2016, 2020](#),
 71 [Allen et al., 2015, 2019](#)]. Next to the most frequently used calibration based on *C. wuellerstorfi*,
 72 there also exist data for another epifaunal species, *C. mundulus*, confirming a relationship
 73 between shell B/Ca and deep seawater $\Delta[\text{CO}_3^{2-}]$, but the calibration shows a different slope,
 74 indicating that the incorporation of B into the shell calcite is affected by species-specific
 75 processes. Therefore, the B/Ca method can only be applied where the same species occurs
 76 throughout the studied interval and also where a sufficient number of shells can be recovered to
 77 facilitate the chemical analysis. This prevents applications in settings where the regional
 78 environmental change caused large shifts in food availability and bottom water oxygen content,
 79 resulting in shifts in benthic communities, as well as in settings with high sedimentation rate,
 80 where the concentration of foraminifera shells is low (e.g. [Kitazato et al., 2000](#), [Gooday, 2003](#),
 81 [Geslin et al., 2004](#)).

82 Planktonic foraminifera shells are a primary component of carbonate in the deep-sea
 83 sediment ([Schiebel, 2002](#)), and the preservation of these shells is intimately associated with the
 84 deep seawater $\Delta[\text{CO}_3^{2-}]$ (e.g., [Berger et al., 1982](#)). Therefore, another way to reconstruct deep
 85 seawater $[\text{CO}_3^{2-}]$ is by the quantification of the degree of dissolution of planktonic foraminifera
 86 shells (e.g. [Berger et al., 1982](#)). Previous studies made use of this relationship, but applied
 87 different ways to quantify dissolution intensity, such as by shell fragmentation, proportion of
 88 dissolution resistant species or the ratio between benthic and planktonic foraminifera ([Berger et
 89 al., 1982](#), [Peterson and Prell, 1985](#), [Kucera, 2007](#)). These proxies all show the expected direction
 90 of the relationship with deep seawater $\Delta[\text{CO}_3^{2-}]$, but are either hard to objectively quantify or are
 91 affected by initial conditions (assemblage composition) ([Kucera, 2007](#)). The size-normalized
 92 weight of sedimentary shell was proposed to quantify carbonate dissolution intensity more
 93 objectively ([Lohmann, 1995](#), [Broecker and Clark, 2001](#)). However, the initial weight of the
 94 planktonic foraminifera shell is also controlled by surface water properties, such as surface water
 95 carbonate chemistry (e.g., [Barker and Elderfield, 2002](#); [Marshall et al., 2013](#)) making
 96 quantitative reconstructions of deep-water $[\text{CO}_3^{2-}]$ impossible in settings where surface
 97 properties have changed as well.

98 More recent studies suggested that the problem of quantifying preservation state of
 99 planktonic foraminifera shells can be circumvented by measurements of shell architecture using
 100 X-ray micro-CT scanning ([Johnstone et al., 2010](#), [Iwasaki et al., 2015](#), [Iwasaki et al., 2019](#)). In
 101 particular, the quantification of shell preservation by measuring the proportion of more strongly
 102 dissolved calcite, identified by their lower CT number, provides a means to objectively
 103 determine the preservation state in a way that is not dependent on the initial size or weight of the
 104 shell. As long as the ratio of the different types of calcites, making up the lamellar structure of
 105 the shells remains the same, the proportion of the more dissolved calcite should only be related
 106 to deep-water $[\text{CO}_3^{2-}]$ ([Iwasaki et al., 2015](#), [Iwasaki et al., 2019](#)). However, so far only a regional
 107 South pacific calibration of the CT-based proxy exists ([Iwasaki et al., 2022](#)). This calibration is
 108 based on a limited number of data points, covering mainly low saturation state waters, and it has
 109 not been directly compared with the B/Ca proxy.

110 In addition, there are factors other than deep seawater $[\text{CO}_3^{2-}]$ variation that control
 111 carbonate dissolution on the deep seafloor and which may affect the CT-based proxy differently
 112 than the B/Ca proxy. The first factor is the variation in sedimentation rate, which alters the
 113 exposure time to deep seawater and results in differences in dissolution intensity of planktonic
 114 foraminifera shells ([Berger et al., 1982](#)). The second factor is the decomposition of organic
 115 material in the sediment, which decreases ambient seawater (or porewater) $[\text{CO}_3^{2-}]$ and may

cause carbonate dissolution in seafloor sediments deposited above the regional lysocline (Berger et al., 1970, Milliman, 1993, Hales and Emerson, 1996, Hales, 2003). Finally, it is known from earlier attempts to use the preservation of planktonic foraminifera shells as a proxy for deep-water properties that significant changes in preservation are only encountered below a certain critical threshold value of deep seawater $[CO_3^{2-}]$, and shells deposited above this foraminiferal lysocline all appear well preserved (Berger et al., 1982). Therefore, to develop the method using CT-scanning of planktonic foraminiferal shells as paleo-deep seawater $[CO_3^{2-}]$ proxy, assessing the effect of these secondary factors on the preservation state of shells deposited in various sedimentary settings is necessary.

To assess the accuracy and reliability of the CT-based proxy for deep seawater $[CO_3^{2-}]$ reconstruction, we have quantified planktonic foraminifera shell preservation in a collection of samples from the South Atlantic, covering a gradient towards higher ambient $\Delta[CO_3^{2-}]$ values, and representing different sedimentation rates and productivity regimes. Importantly, in all the analyzed samples, B/Ca of *C. wuellerstorfi* have been determined by (Rae et al., 2011, Raitzsch et al., 2013), allowing direct proxy intercomparison. We quantified the degree of shell dissolution in four planktonic foraminifera species (*G. bulloides*, *G. inflata*, *G. ruber*, and *T. sacculifer*) and propose a new way to quantify the proportion of more dissolved calcite, which does not require instrument-specific calibration of the strength of the X-ray beam. We combine the new measurements with previously obtained CT images (Iwasaki et al., 2019, 2022) to determine the regional and species-specific effects and establish a new calibration formula, allowing reconstructions of deep seawater $\Delta[CO_3^{2-}]$.

137

138 2 Materials and Methods

139 2.1. Multiple core samples and physicochemical properties

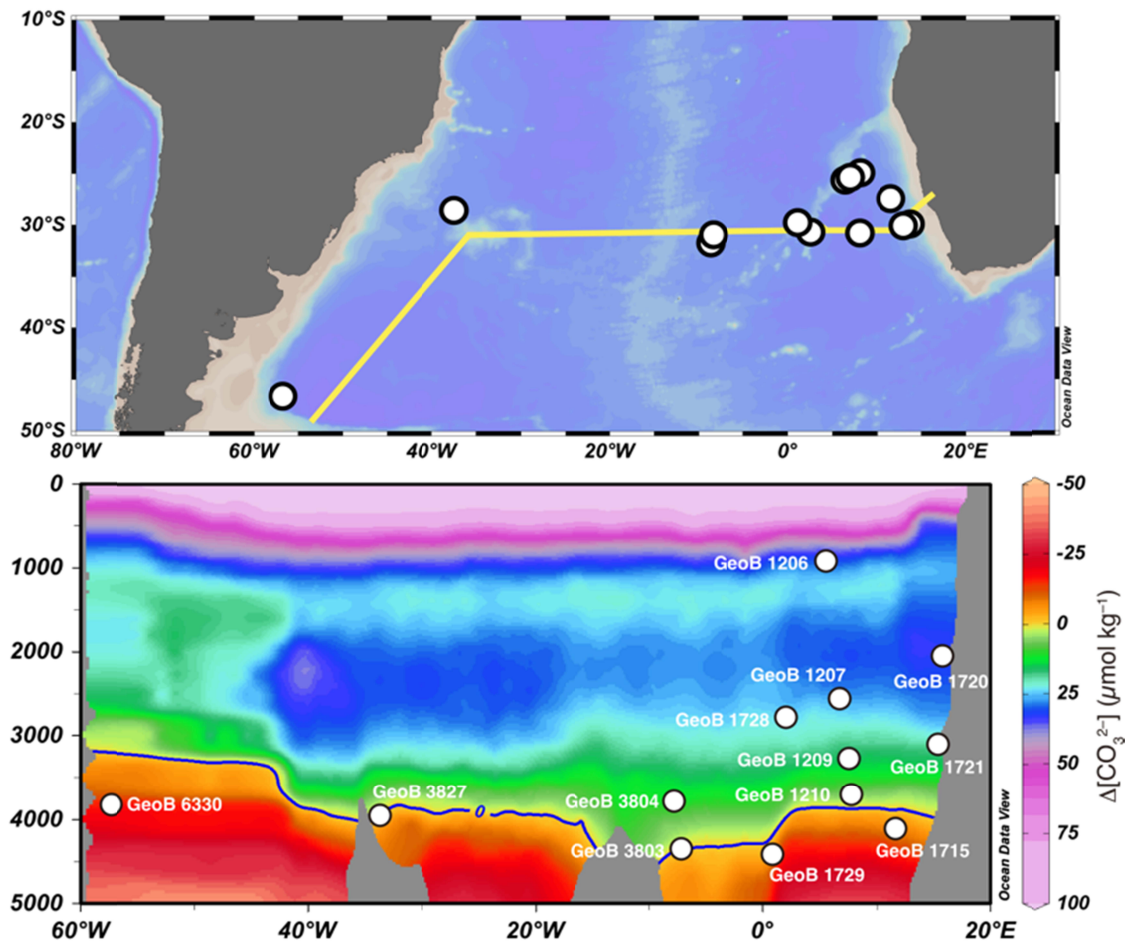
140 In this study, we used planktonic foraminifera shells extracted from 13 core top samples
 141 collected by multiple corer between 940 and 4173 m water depth in the South Atlantic (Figure
 142 1). The samples represent a subset of core tops where benthic foraminiferal (*Cibicidoides*
 143 *wuellerstorfi*) B/Ca ratio, a conventional proxy of deep seawater $[CO_3^{2-}]$, has been determined
 144 by previous studies (Rae et al., 2011, Raitzsch et al., 2013) (Figure 2). The subset contains all
 145 samples used in the previous studies for which the material is stored in the GeoB repository in
 146 Bremen and where information is available on sedimentation rate and accumulation rate of
 147 organic carbon. From each core top sample, eight shells of each of four planktic foraminiferal
 148 species (*G. bulloides*, *G. inflata*, *G. ruber*, and *T. sacculifer*) were collected for analysis by X-ray
 149 micro-CT scanning. Among the 13 sites, shells of *G. bulloides* could be collected from all sites,
 150 shells of *G. inflata* and *T. sacculifer* were collected from 12 sites, and shells of *G. ruber* were
 151 collected from 11 sites. The all shells were collected from the 300-355 μm size fraction, and are
 152 not fragmented or containing fractures and holes, or peeling of the surface. Estimates of
 153 sedimentation rate ($cm\ kyr^{-1}$) at the studied sites were taken from age models of sediment cores
 154 sampled at the same site (Wefer et al., 1990, Schulz et al., 1992, 1996; Bleil et al. 2001), and
 155 used to calculate accumulation rate of organic carbon ($g\ cm^{-2}\ kyr^{-1}$) making use of total organic
 156 carbon content (%TOC) and dry bulk density ($g\ cm^{-3}$) data for each site (Mollenhauer et al.,
 157 2004).

158 In addition to the above sample set, we used a subset of published 16 core top samples
 159 from the Pacific Ocean to extend the dissolution intensity calibration over a larger range of deep

160 seawater $\Delta[\text{CO}_3^{2-}]$ values (Iwasaki et al., 2019, 2022). The core top sediment samples were
 161 obtained by multiple core sampling from the water depth between 1500 and 4000 m, with most
 162 of them located below the dissolution transition depth level ($\Delta[\text{CO}_3^{2-}] < 10 \mu\text{mol kg}^{-1}$). From
 163 each core top sample, more than eight shells of each of three planktic foraminiferal species (*G. bulloides*,
 164 *G. ruber*, and *T. sacculifer*) without external damage were collected from 200–355 μm
 165 size fraction for analysis by X-ray micro-CT scanning in previous studies, and the existing scans
 166 were here used for the calculation of the newly defined CT based dissolution index (Iwasaki et
 167 al., 2019 and 2022). To remain consistent with the existing data and due to the difficulty to
 168 unambiguously and consistently separating both species (Morard et al., 2019), specimens
 169 designated as *G. ruber* may contain both *G. ruber albus* and *G. elongatus*.

170 Bottom water values of $\Delta[\text{CO}_3^{2-}]$ for all of studied sites were calculated from
 171 physicochemical parameters (temperature, salinity, total alkalinity, total inorganic carbon, and
 172 concentrations of phosphate and silicate) measured at nearby Global Ocean Data Analysis
 173 Project (GLODAP) profiles (Key et al., 2004). The site information and the estimated values of
 174 bottom water physicochemical properties for all Atlantic and Pacific sites are summarized in
 175 **Table 1**.

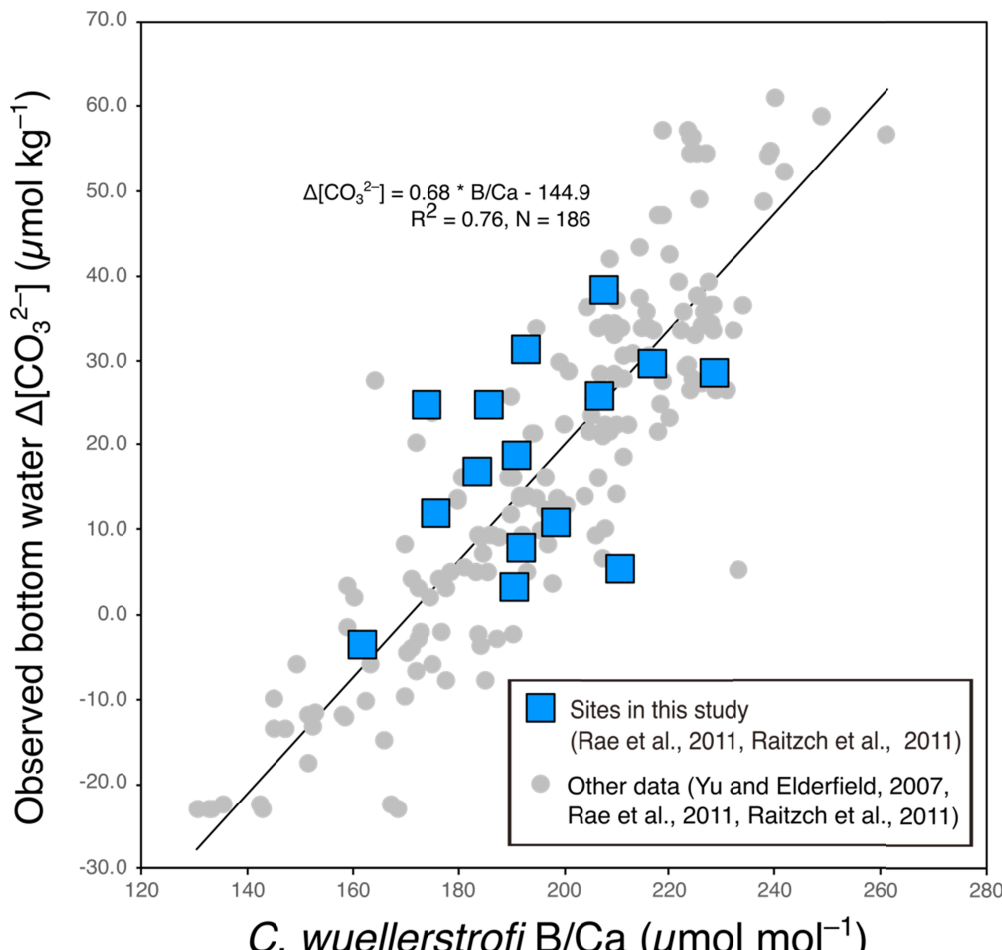
176



177
 178 Figure 1. The locations of multiple corer samples in the South Atlantic used in this study. The
 179 section along the yellow line is showing the spatial distribution of the degree of carbonate
 180 saturation ($\Delta[\text{CO}_3^{2-}]$) in the study area.

181

182



183

$C. \text{wuellerstrofi}$ B/Ca ($\mu\text{mol mol}^{-1}$)

Figure 2. B/Ca ratio in shells of the benthic foraminifera *Cibicidoides wuellerstorfi* in core top samples plotted against deep-water $\Delta[\text{CO}_3^{2-}]$. The data of B/Ca ratio of benthic foraminifera in the core-top sample used in this study are shown by blue squares. Data are derived from Rae et al. (2011), Raitzsch et al. (2011), and Yu and Elderfield (2007).

188

189

Cruise	Site	Latitude (S)	longitude (W)	Depth (m)	Deep water $\Delta[\text{CO}_3^{2-}]$ ($\mu\text{mol kg}^{-1}$)	Linear Sedimentation Rate (cm kyr^{-1})	TOC accumulation rate ($\text{g m}^{-2} \text{y}^{-1}$)	Caronate content (%)	$C. \text{w.B/Ca}$ ($\mu\text{mol mol}^{-1}$)	error
M 12/1	1206-1	24.67	-6.48	940	25.1	No data	No data	No data	193	4
M 12/1	1207-2	24.59	-6.85	2593	29.9	1.5	0.17	95.5	217	7
M 12/1	1209-1	24.50	-7.28	3303	14.6	3.3	0.41	95.9	191	9
M 12/1	1210-3	24.48	-7.43	3750	6.5	1.4	0.16	93.7	192	5
M 20/2	1715-1	26.47	-11.63	4097	-5.9	10.0	1.73	83.0	191	8
M 20/2	1720-3	29.00	-13.82	2004	33.2	6.0	3.30	78.8	208	9
M 20/2	1721-5	29.17	-13.08	3045	18.9	6.0	1.41	84.8	186	9
M 20/2	1728-3	29.83	-2.40	2887	23.8	2.0	0.30	94.9	229	7
M 20/2	1729-1	28.88	-1.00	4401	-0.1	0.6	0.08	93.6	211	6
M 34/3	3803-1	30.34	8.57	4173	3.1	0.8	0.16	90.0	199	10
M 34/3	3804-2	30.74	8.77	3882	7.8	0.7	0.12	92.2	184	10
M 34/3	3827-1	25.02	38.54	3842	-4.3	0.9	0.18	50.5	176	9
M 46/3	6330-1	46.15	57.56	3874	-13.1	No data	No data	No data	162	7

190

191

192

193

194

Table 1: Multiple core sample locations, depth (m), Deep water degree of $\Delta[\text{CO}_3^{2-}]$ ($\mu\text{mol kg}^{-1}$), Linear Sedimentation Rate (cm kyr^{-1}), TOC (Total Organic Carbon) accumulation rate ($\text{g m}^{-2} \text{y}^{-1}$) and *Cibicidoides wuellerstorfi* B/Ca ratio ($\mu\text{mol mol}^{-1}$) at each sampling site.

195 **2.2. X-ray Micro-CT Scanning**

196 The XMCT system (ScanXmate-D160TSS105/11000, WhiteRabbit Corp., Tokyo, Japan) at
 197 the Japan Agency for Marine-Earth Science and Technology, Yokosuka, Japan, was used to
 198 obtain three-dimensional X-ray images of foraminiferal shells. The imaging was carried out with
 199 a high-resolution setting (X-ray focus spot diameter, 0.8 μm ; X-ray tube voltage, 80 kV; detector
 200 array size, 2000 \times 1336; 1500 projections/360°; 0.5 s/projection). After XMCT scanning,
 201 ConeCTexpress software (WhiteRabbit Corp., Tokyo, Japan) was used to convert the raw
 202 tomography data into segmented images of foraminifera shells. Image cross-sections were
 203 reconstructed from filtered back projections following the general principle of Feldkamp cone-
 204 beam reconstruction. The scanning and data processing methods followed a previous study
 205 [Iwasaki et al., 2015]. The CT number, indicating calcite density and visualizable porosity, was
 206 calculated based on the X-ray attenuation coefficient of each sample. We used Molcer Plus 3-D
 207 imaging software (WhiteRabbit Corp., Tokyo, Japan) to obtain isosurface images of the shells.
 208 Then, we evaluated the CT number histograms of each shell based on the 3-D tomography data.

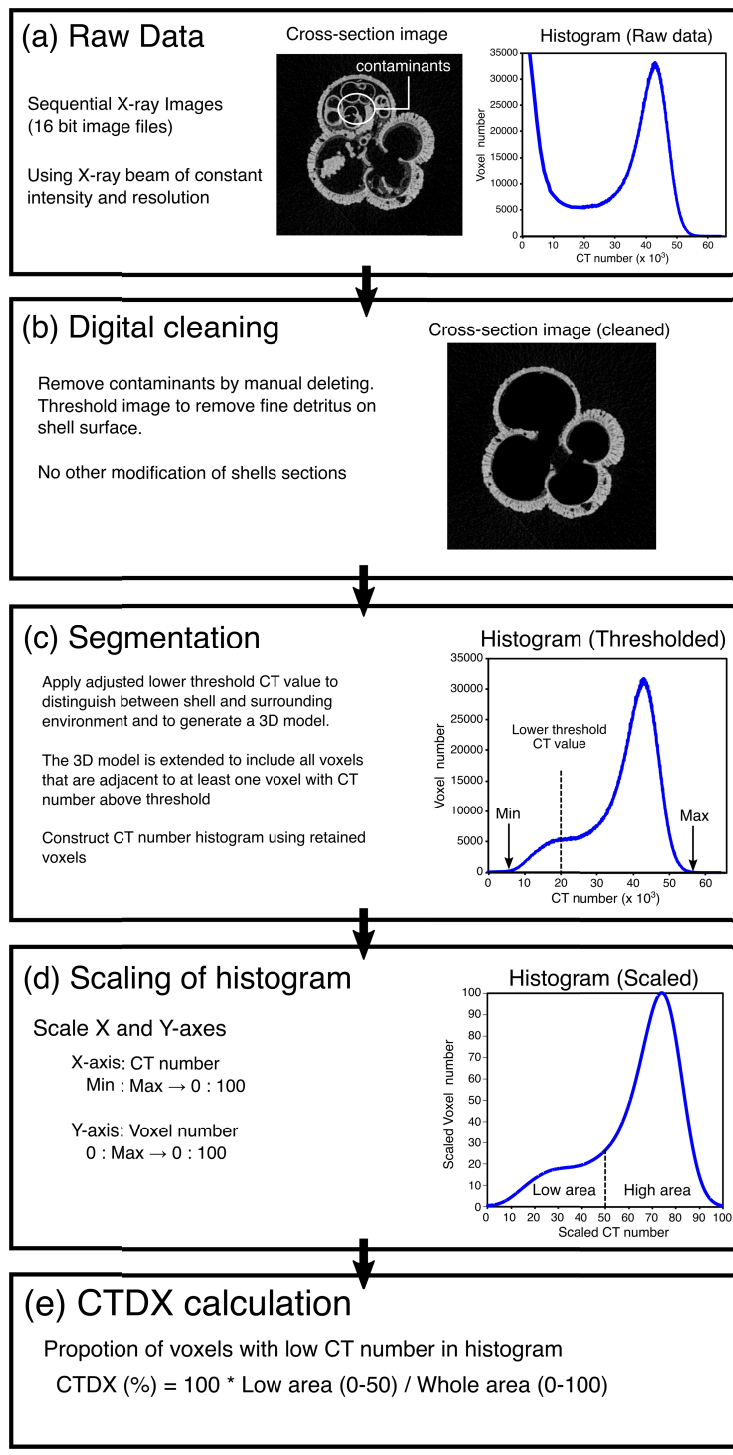
210 **2.3. Protocol of CT data processing for calculating CTDX**

211 The CT scanning-based dissolution index (CTDX) of the planktic foraminiferal test
 212 employed in this study follows the same concept as the proxy of %Low-CT-number calcite
 213 volume previously suggested (Iwasaki et al., 2019, 2022). However, in this study, we modify the
 214 %Low-CT-number calcite volume proxy in a way that the resulting value is not dependent on the
 215 exact settings of the scanner, enabling applications using other X-ray micro-CT scanners, which
 216 had been modified to remove beam-hardening effects for assessing quantitative bulk density (i.e.
 217 submicron scale porosity) of organic carbonate. The protocol to calculate the value of CTDX
 218 from Serial Cross-Sectional Images of each specimen is shown in Figure 3. First, from the initial
 219 raw data (sequential sectional images) (Figure 3a), contaminants (e.g., detritus, fragments and
 220 other small foraminifera shells) stuck inside the test were removed by manual digital image
 221 processing (Figure 3b). After that, to segment shell material from other environments, we
 222 determined the lower threshold CT value by visual inspection of multiple specimens, ensuring
 223 only shell material is included. Under the process of segmentation, to facilitate a replicable
 224 smoothing of the shell surface and to make sure all voxels attached to the shell surface are
 225 included, we introduce a step where the six-neighboring voxels of a voxel located on the air-
 226 calcite boundary are retained. This is important to maintain voxels that partially contain shell
 227 material for the analysis. CT values in voxels retained after cleaning, segmentation, and
 228 thresholding were used to generate a CT histogram of the foraminiferal shell that could be used
 229 to calculate the dissolution index (Figure 3c). Previous studies [Iwasaki et al. 2019, 2022]
 230 suggested that the CT number histogram changes from monomodal to bimodal distribution with
 231 increasing dissolution. Based on this characteristic of change in the histogram shape with test
 232 dissolution, they proposed the relative volume of low-CT-number calcite to the volume of calcite
 233 in the whole shell (%Low-CT-number calcite volume) as a quantitative carbonate dissolution
 234 proxy for dissolution. Here we build on this approach but develop a new Dissolution Index
 235 (CTDX), which defines the threshold CT value independently of the scanner setting, using the
 236 shape of the CT value histogram. To this end, we first scaled the original CT number histogram
 237 by assigning 0 and 100 to the voxels with the lowest and highest CT values (Figure 3d). After
 238 that, we calculated the CTDX as the area ratio of the lower part of the histogram (X-axis: 0-50)
 239 to the whole histogram (X-axis: 0-100) (Figure 3e). Finally, we assigned a CTDX value to a
 240 sample as the average CTDX value of at least eight individual specimens. The minimum number

241 of shells needed to provide a representative estimate of the average preservation state of a given
 242 foraminifera species was determined by [Iwasaki et al. \(2022\)](#).

243

244



245

246

247

248

Figure 3. The protocol to calculate the foraminiferal shell dissolution index (CTDX) starts from raw sequential X-ray image data (a). (b) Contaminants in the shell sample are removed by manual deleting. (c) Apply threshold to distinguish between calcite material and surrounding

249 environment. Extract CT number histogram from cleaned and threshold 3D data. (d) Scaling X
 250 and Y-axes of CT number histogram. (e) Calculation of CTDX (%).

251

252 3 Results

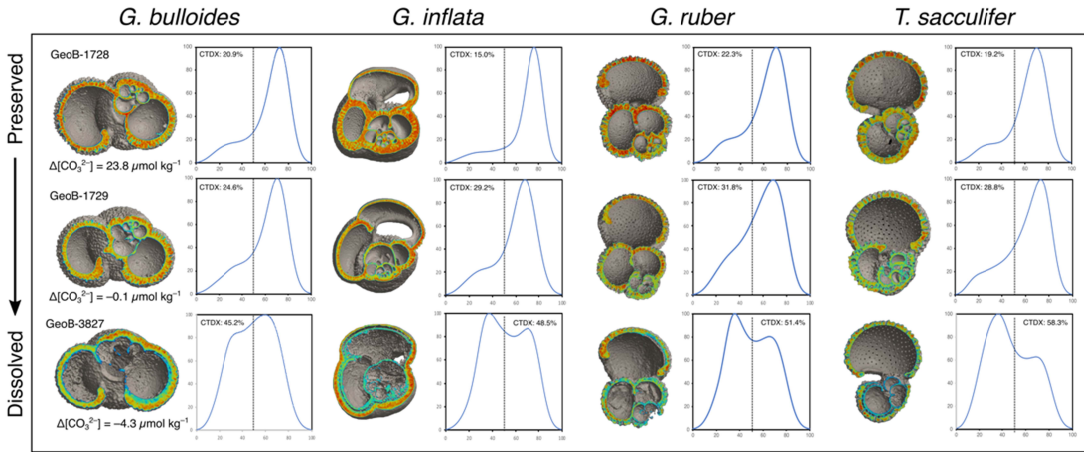
253 3.1. Evaluating test dissolution by X-ray micro-CT scanning

254 The X-ray micro-CT scanning enables us to observe the internal structure of the
 255 foraminiferal shell and calcite density distribution in a single specimen's shell. The CT number
 256 histogram provides an objective and quantitative means to evaluate microscale calcite density
 257 distribution in each specimen. The [Figure 4](#) shows the changes in the internal shell structure and
 258 CT number histogram of four species of planktic foraminifera in three seafloor sediment samples
 259 representing different locations and bottom water $\Delta[\text{CO}_3^{2-}]$ conditions. As expected, and in
 260 agreement with previous studies ([Johnson et al., 2010](#), [Iwasaki et al., 2019](#)), we find a
 261 progression of shell dissolution with decreasing $\Delta[\text{CO}_3^{2-}]$. The dissolution first affects the septa
 262 among the juvenile chambers and then spreads to the inner layer of the chambers in the final
 263 whorl. With progressive dissolution, the CT number histograms show a shift from a unimodal
 264 distribution with a single, high CT number peak to a bimodal distribution, followed by a trend
 265 toward a unimodal density distribution with a peak at a low CT number. These are consistent
 266 with the results of previous studies ([Iwasaki et al., 2015, 2019](#)), suggesting that the shape of the
 267 CT number histogram, irrespective of the CT scanning settings, can be used to describe the
 268 preservation state of the foraminiferal shell.

269 Assuming that the shape of the CT number histogram, converted to the CTDX value as
 270 described above, quantify the degree of shell alteration due to selective dissolution (removal) of
 271 the most susceptible parts of the shell, the CTDX-based average state of shells of a given species
 272 of planktonic foraminifera should show a systematic relationship with deep-water chemistry.
 273 This is important, because the CTDX value is independent of the size and shape of the analyzed
 274 individual shells. It describes the portion of the shell that is affected by dissolution, irrespective
 275 of the analyzed calcite volume. In theory, the CTDX could even be applied to multiple species of
 276 foraminifera, but because the shell architectures among species vary significantly, we began by
 277 comparing the *G. bulloides* CTDX with that of three other species (*G. ruber*, *T. sacculifer*,
 278 and *G. inflata*) in the same sediment samples to also evaluate the inter-species variation in
 279 CTDX ([Figure 5](#)). The results shows that CTDX of *G. bulloides* significantly correlates with the
 280 other three species (*G. ruber*: $R^2 = 0.7$, *T. sacculifer*: $R^2 = 0.72$, *G. inflata*: $R^2 = 0.81$), suggesting
 281 that the CTDX of each of the species should be applicable as a dissolution proxy. However, the
 282 CTDX values among the species are offset, in particular for the relationship between CTDX of
 283 *G. bulloides*, *T. sacculifer* and *G. inflata*, the slopes of regression lines are relatively high (*T.*
 284 *sacculifer*: 1.69, *G. inflata*: 1.39). This implies that *T. sacculifer* and *G. inflata* are more sensitive
 285 to dissolution expressed by the CTDX index than *G. bulloides*.

286

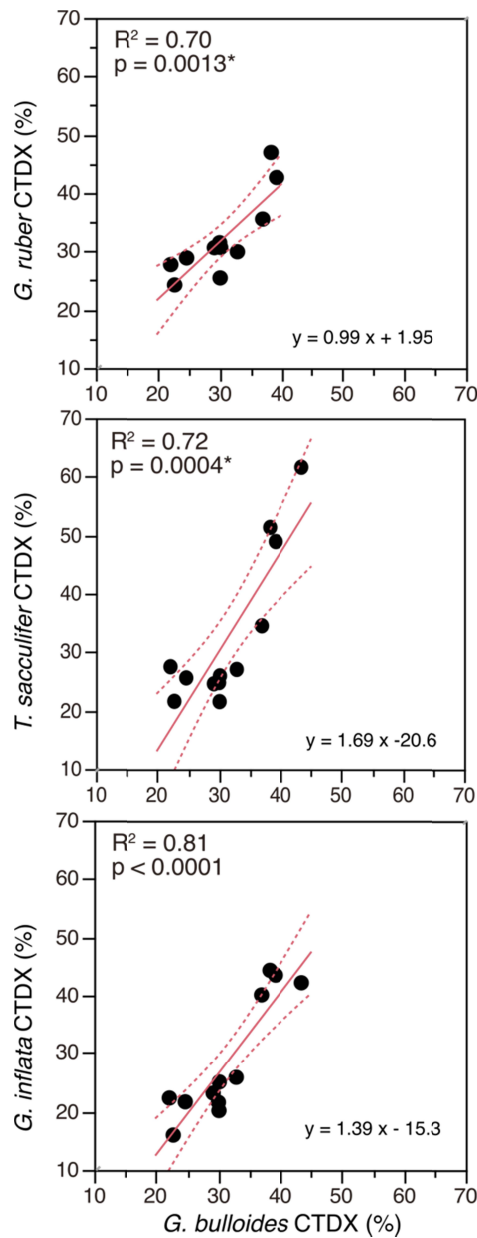
287



288
289 Figure 4. Changes in cross-sectional isosurface images and CT number histograms of four major
290 species of planktonic foraminiferal shells (*G. bulloides*, *G. inflata*, *G. ruber* and *T. sacculifer*)
291 with the progression of dissolution. Shells were obtained from three core top samples (GeoB-
292 1728, 1729, and 3827). The condition of selected tests, which have CTDX similar to average of
293 each sample set, are shown. $\Delta[\text{CO}_3^{2-}]$ at the nearest GLODAP stations at the core-top sample
294 depths ranged from -4.3 to $23.8 \mu\text{mol kg}^{-1}$. The dashed line in the CT number histograms shows
295 the threshold (50) between low and high values.

296

297

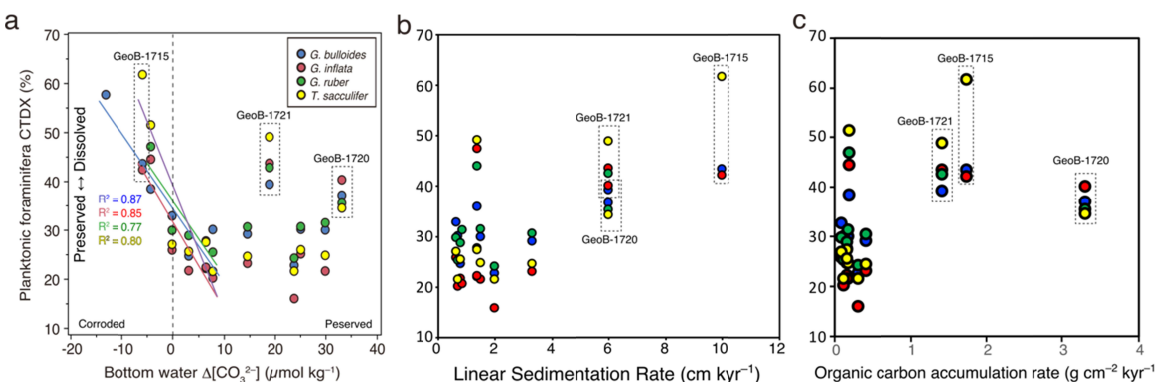


298
299 Figure 5. Inter species comparison of *G. bulloides* CTDX with other three species obtained from
300 same core-top samples. The square of the correlation coefficient (R^2) and the type I error rate (p -
301 value) are also shown.
302

303 **3.2. Comparison between planktonic foraminiferal CTDX, bottom water $\Delta[\text{CO}_3^{2-}]$, MAR,
304 and organic carbon flux**

305 To assess the main controlling factors on foraminifera shell dissolution on the deep seafloor,
306 we compared the planktonic foraminiferal shell CTDX values as a carbonate dissolution index,
307 with three parameters: Bottom water $\Delta[\text{CO}_3^{2-}]$ representing ambient seawater corrosiveness,
308 Linear Sedimentation Rate describing the exposure time of the shells on the seafloor, and
309 Organic carbonate accumulation rate approximating supralysocinal dissolution due to elevated
310 porewater CO₂ from organic matter remineralization, for the 13 Atlantic samples where all
311 parameters were available (Figure 6). First, we found a significant correlation between the

312 planktonic foraminiferal CTDX and the bottom water $\Delta[\text{CO}_3^{2-}]$ under the low $\Delta[\text{CO}_3^{2-}]$
 313 condition ($< 10 \mu\text{mol kg}^{-1}$): *G. bulloides*; $R^2 = 0.87$, *G. inflata*; $R^2 = 0.85$, *G. ruber*; $R^2 = 0.77$, *T.*
 314 *sacculifer*; $R^2 = 0.80$ (Figure 6a). In contrast, the comparison between CTDX and sedimentation
 315 rate site did not show any support for the hypothesis that higher sedimentation rate facilitates
 316 better preservation of carbonate by faster burial (Figure 6b). These results suggest that the
 317 carbonate dissolution intensity in the South Atlantic is generally governed by bottom water
 318 $\Delta[\text{CO}_3^{2-}]$ under low $\Delta[\text{CO}_3^{2-}]$ condition ($< 10 \mu\text{mol kg}^{-1}$), not by sedimentation rate. Under high
 319 $\Delta[\text{CO}_3^{2-}]$ conditions ($> 10 \mu\text{mol kg}^{-1}$), high CTDX values are observed at two sites (GeoB 1720
 320 and 1721), suggesting significant dissolution of carbonate, despite the supersaturated conditions
 321 for calcite in the ambient seawater. Here, a comparison with organic carbon accumulation rate ($\text{g cm}^{-2} \text{kyr}^{-1}$) reveals that the organic carbon inputs at both sites is more than three times higher
 322 than at the other sites (Figure 6c). These results indicate that organic carbon decomposition in the
 323 seafloor sediment may affect preservation of planktonic foraminifera shells even under
 324 supralysoclinal conditions ($> 10 \mu\text{mol kg}^{-1}$).
 325
 326
 327

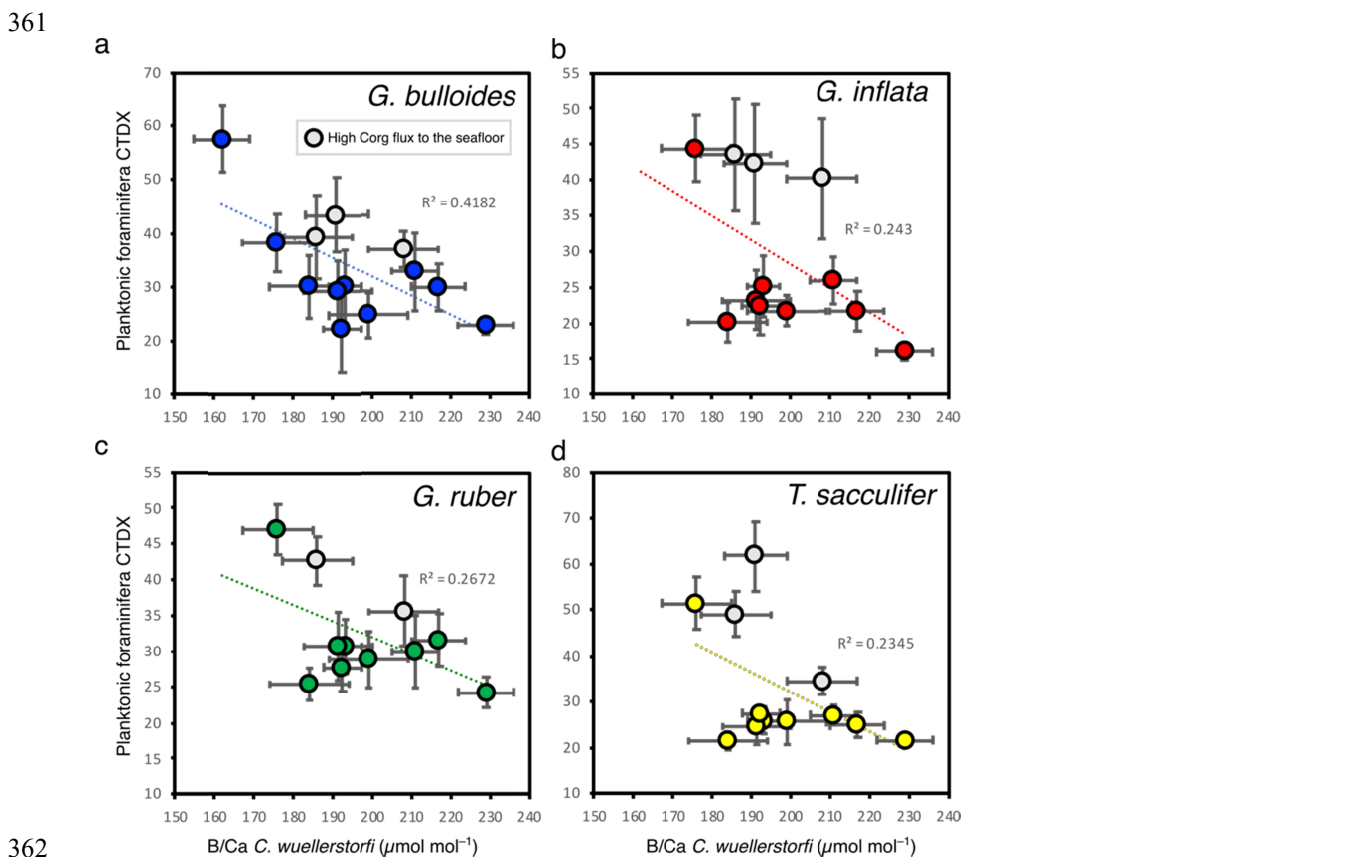


328
 329 Figure 6. Investigation in controlling factor of foraminiferal shell dissolution intensity. (a)
 330 Bottom water $\Delta[\text{CO}_3^{2-}] (\mu\text{mol kg}^{-1})$, (b) Liner Sedimentation Rate (cm kyr^{-1}), and (c) Organic
 331 carbon accumulation rate ($\text{g cm}^{-2} \text{kyr}^{-1}$) versus Planktonic foraminifera CTDX (%) at each
 332 sampling site. The data points at the sites locate in the Benguela upwelling system (GeoB-1715,
 333 1720 and 1721) with high organic carbon accumulation rate are surrounded by dotted line.
 334

3.3. Comparison with the proxy of benthic foraminiferal B/Ca ratio

335 To investigate the applicability of the CTDX as a deep seawater $\Delta[\text{CO}_3^{2-}]$ proxy, we next
 336 compared the CTDX values in the 13 South Atlantic samples with the B/Ca ratio of benthic
 337 foraminifera (*C. wuellerstorfi*) (Figure 7). The B/Ca ratio of benthic foraminifera (*C.*
 338 *wuellerstorfi*), a conventional quantitative proxy of deep seawater $\Delta[\text{CO}_3^{2-}]$, derived from the
 339 same sediment samples showed a weak correlation with the CTDX of each species: *G. bulloides*;
 340 $R^2 = 0.42$, $p = 0.0169^*$, *G. inflata*; $R^2 = 0.24$, $p = 0.1034$, *G. ruber*; $R^2 = 0.27$, $p = 0.1034$, *T.*
 341 *sacculifer*; $R^2 = 0.28$, $p = 0.0960$ (Figure 7). The correlation has in all cases the expected sign
 342 (both proxies indicating more dissolution in the same samples), but the observation that the
 343 CTDX and B/Ca ratio correlation is not as pronounced as the correlation between CTDX and the
 344 bottom water $\Delta[\text{CO}_3^{2-}]$ is puzzling. Next, we focused on the *G. bulloides* CTDX, because this
 345 species was found at all sites, and showed the most significant correlation with the benthic
 346 foraminiferal B/Ca ratio among four species. The Figure 8 shows the relationship between two
 347

348 proxies (*G. bulloides* CTDX and benthic foraminifera B/Ca ratio) and the bottom water $\Delta[\text{CO}_3^{2-}]$
 349 under the lower deep seawater $\Delta[\text{CO}_3^{2-}]$ condition ($< 10 \mu\text{mol kg}^{-1}$). Based on this comparison,
 350 we identified the sites where either proxy is discrepant, and investigated the factors that may be
 351 responsible for the discrepancy in these two proxies. In this plot, the regression lines between *G.*
 352 *bulloides* CTDX and bottom water $\Delta[\text{CO}_3^{2-}]$ obtained from the results of this study and that
 353 between the benthic foraminiferal B/Ca ratio and bottom water $\Delta[\text{CO}_3^{2-}]$ obtained from the
 354 results of calibration using more than 200 core-top samples (Yu et al., 2013) were presented. The
 355 result shows that the benthic foraminiferal B/Ca ratio is at least $20 \mu\text{mol mol}^{-1}$ higher than the
 356 regression line at two sites: Site 1715 (Depth: 4097 m, bottom water $\Delta[\text{CO}_3^{2-}]$: $-5.87 \mu\text{mol kg}^{-1}$);
 357 Site 1729 (Depth: 4401 m, bottom water $\Delta[\text{CO}_3^{2-}]$: $-0.10 \mu\text{mol kg}^{-1}$). At those sites, the
 358 estimated value of bottom water $\Delta[\text{CO}_3^{2-}]$ derived from the benthic foraminiferal B/Ca ratio
 359 imply higher than observed $\Delta[\text{CO}_3^{2-}]$.
 360



362
 363
 364 Figure 7. Relationship between planktonic foraminiferal CTDX of (a) *G. bulloides*, (b) *G.*
 365 *inflata*, (c) *G. ruber*, and (d) *T. sacculifer* and B/Ca ratio of *C. wuellerstorfi* ($\mu\text{mol mol}^{-1}$) in each
 366 core-top sample. The sampling sites located in the Benguela upwelling system with high organic
 367 carbon flux are shown by gray circle. The regression line and the square of the correlation
 368 coefficient (R^2) are also shown.
 369
 370

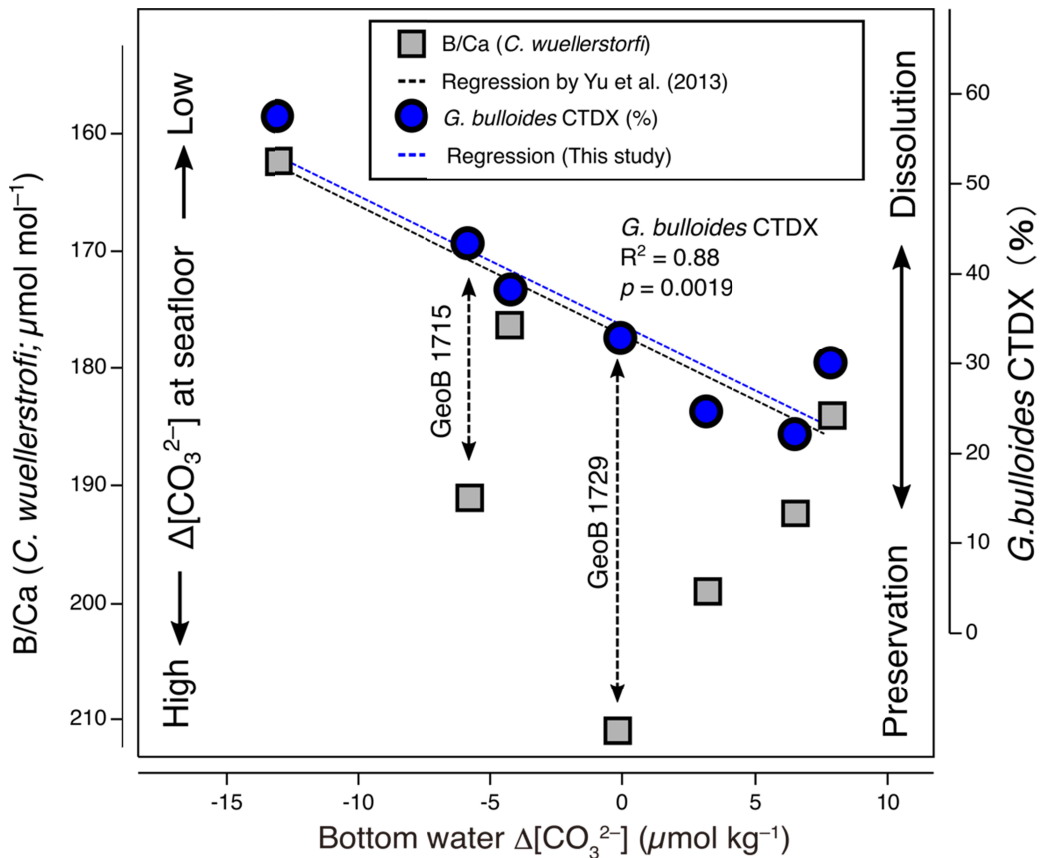


Figure 8. Comparison of the plots of *G. bulloides* CTDX and B/Ca ratio of *C. wuellerstorfi* against bottom seawater $\Delta[\text{CO}_3^{2-}]$ under the condition of low bottom seawater $\Delta[\text{CO}_3^{2-}]$ ($< 10 \mu\text{mol kg}^{-1}$). The B/Ca ratio of *C. wuellerstorfi* at the site GeoB-1715, 1729 and 3803 are relatively higher than *G. bulloides* CTDX.

3.4. Extended calibration between CTDX and deep water $\Delta[\text{CO}_3^{2-}]$

In addition to the 13 core top samples collected in the South Atlantic, we added the 16 core top samples collected in the Pacific Ocean to assess the behavior of the CTDX proxy under the condition of low deep seawater $\Delta[\text{CO}_3^{2-}]$ ($< 10 \mu\text{mol kg}^{-1}$) and to obtain an extended calibration equation between CTDX and deep seawater $\Delta[\text{CO}_3^{2-}]$ in the wider range of global ocean. The plot shows the relationship between the CTDX of three species of major planktic foraminiferal shell (*G. bulloides*, *G. ruber* and *T. sacculifer*) and deep water $\Delta[\text{CO}_3^{2-}]$ obtained from nearby bottle water sampling at each site (Figure 9). The sites at GeoB 1720 and 1721, with high organic material deposition, are excluded from the plot. The plot provides the relationship between CTDX and a wide range of deep seawater $\Delta[\text{CO}_3^{2-}]$ (-27 to $30 \mu\text{mol kg}^{-1}$), and suggests that CTDX of each species significantly correlate with deep seawater $\Delta[\text{CO}_3^{2-}]$ between the range of -20 to $10 \mu\text{mol kg}^{-1}$. The results of calibrations in each species are as follows:

$$\text{G. bulloides: Deep seawater } \Delta[\text{CO}_3^{2-}] = -0.65 * \text{CTDX} + 24.8 \quad (R^2 = 0.57, N = 15)$$

$$\text{G. ruber: Deep seawater } \Delta[\text{CO}_3^{2-}] = -0.56 * \text{CTDX} + 20.5 \quad (R^2 = 0.88, N = 12)$$

$$\text{T. sacculifer: Deep seawater } \Delta[\text{CO}_3^{2-}] = -0.43 * \text{CTDX} + 15.3 \quad (R^2 = 0.88, N = 13)$$

395
396
397
398
399
400
401
402
403
404
405

These calibrations revealed that the CTDX of planktonic foraminifera are able to work as deep-water $\Delta[\text{CO}_3^{2-}]$ proxy in the specific range of the deep seawater $\Delta[\text{CO}_3^{2-}]$ (-20 to $10 \mu\text{mol kg}^{-1}$). However, the variation in the slope of regression line for each species indicated that the sensitivity of CTDX to dissolution varied among species. Based on the regression analysis, the uncertainties of the above regression equations are $\pm 5.7 \mu\text{mol kg}^{-1}$ (*G. bulloides*, N = 15), $\pm 2.8 \mu\text{mol kg}^{-1}$ (*G. ruber*, N = 12), and $\pm 2.6 \mu\text{mol kg}^{-1}$ (*T. sacculifer*, N = 13). On the other hand, the CTDX shows stable values of around 25 and 60 under the high ($> 10 \mu\text{mol kg}^{-1}$) and low ($< -20 \mu\text{mol kg}^{-1}$) carbonate saturation state condition, respectively.

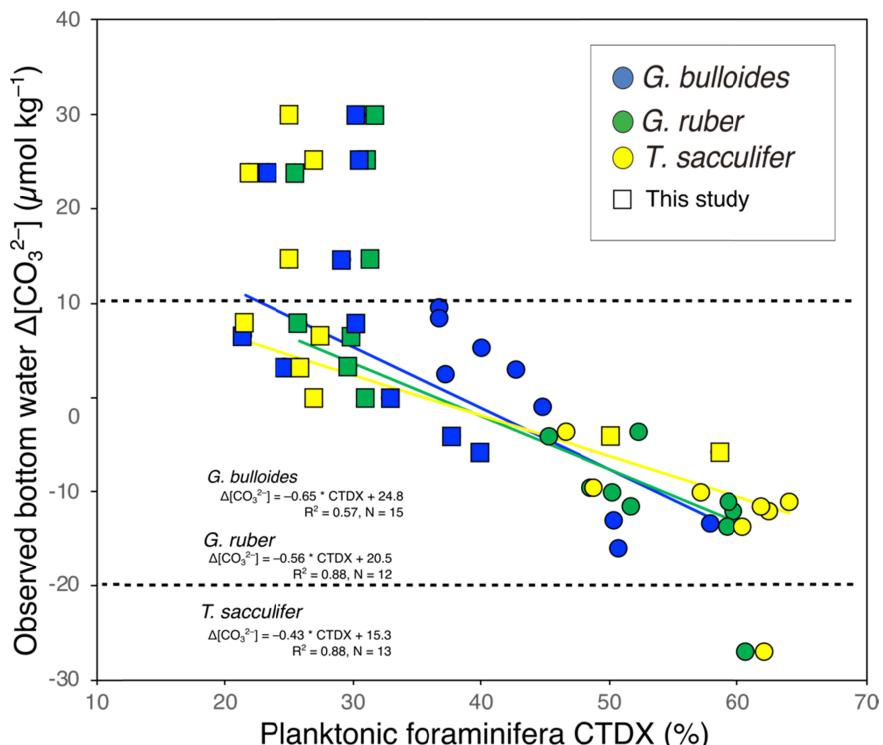
406
407
408
409
410

Figure 9. The CTDX of planktonic foraminifera (*G. bulloides*, *G. ruber* and *T. sacculifer*) in core top samples plotted against deep-water $\Delta[\text{CO}_3^{2-}]$. Core-top samples are obtained from this study and previous studies (Iwasaki et al., 2019 and 2022).

411

4 Discussion

412

4.1 Controlling factors of the planktonic foraminiferal CTDX

413
414
415
416
417
418
419
420

Dissolution of the planktonic foraminiferal shell is considered to occur mainly on deep seafloor under the control of ambient seawater $\Delta[\text{CO}_3^{2-}]$. At the same time, it can be affected by the variance in sedimentation rate and organic carbon respiration at the sediment surface [e.g., Berger et al., 1982, Milliman, 1993]. The direct comparisons between three numerical indexes derived from deep seafloor in this study (i.e., planktic foraminiferal CTDX, bottom water $\Delta[\text{CO}_3^{2-}]$, the sedimentation rate, and the organic carbon accumulation rate at each site) provided the critical information to identify the controlling factor of carbonate dissolution at the deep seafloor. First, the significant correlation between the proxy of CTDX and bottom water $\Delta[\text{CO}_3^{2-}]$

421] proves that dissolution of the planktic foraminiferal shell is undoubtedly controlled by bottom
 422 water $\Delta[\text{CO}_3^{2-}]$ in the most sites under the lower condition of bottom water $\Delta[\text{CO}_3^{2-}]$ ($< 10 \mu\text{mol}$
 423 kg^{-1}). Second, the sedimentation rate is not correlated with the planktic foraminiferal CTDX.
 424 This result suggests that the variance in sedimentation rate, which corresponds to approx. 5-to-
 425 10-fold difference in sedimentation rate does not significantly impact the carbonate dissolution
 426 variance at the deep seafloor. Third, the CTDX showed significantly higher values at two data
 427 sites (GeoB-1720 and 1721) than at the other data points under the condition of higher deep
 428 seawater $\Delta[\text{CO}_3^{2-}]$ ($> 10 \mu\text{mol kg}^{-1}$), which implies the exceeded carbonate dissolution under the
 429 supersaturated condition. These two sites are located at the Benguela Upwelling System in the
 430 eastern South Atlantic, one of the significant continental margins upwelling systems and belongs
 431 to the high productivity area of the ocean [Berger, 1989]. Previous research in the Benguela
 432 Upwelling System suggested that carbonate dissolution occurs at 400-1600 m above the
 433 lysocline by the above process (Vobers and Hinrich, 2002), induced by the release of CO_2 due to
 434 the oxidation of organic material within the sediment (Emerson and Bender, 1981; Archer, 1991;
 435 Jahnke et al., 1994). In addition, the other potential factor is that the porous shell, possibly
 436 response to rapid chamber formation, resulting in the formation of shells that are prone to
 437 dissolution. Culture studies have shown that the chamber formation rate increases under the food
 438 abundant condition as like as upwelling region (Bé et al., 2009), and such high chamber
 439 formation rate could provide the porous shell formation (Berger, 1970). In either case, we
 440 consider that the observed dissolution of planktonic foraminifera shells in the sediments derived
 441 from the Benguela Upwelling System in this study is not controlled by deep seawater $\Delta[\text{CO}_3^{2-}]$,
 442 but was probably brought by other factors such as decomposition of organic material occurring
 443 above the regional lysocline and ontogenetic growth condition at sea surface.

444 On the other hand, the relationship between benthic foraminiferal B/Ca ratio and deep-
 445 water $\Delta[\text{CO}_3^{2-}]$ did not show any unusual values at the sites from the Benguela Upwelling
 446 System, suggesting that the organic material decomposition does not have notable impact on
 447 benthic foraminiferal B/Ca ratio. We suppose that the reduction in seawater $\Delta[\text{CO}_3^{2-}]$, caused by
 448 organic material decomposition, has a more substantial influence on the dissolution of the
 449 planktonic foraminiferal test than the reduction in the B/Ca ratio of the benthic foraminiferal test.
 450 The mechanism to explain these results is to hypothesize that the decrease in seawater $\Delta[\text{CO}_3^{2-}]$
 451 due to organic material decomposition occurs mainly inside the sediment or aggregates of
 452 organic material like marine snow or fecal pellets. Such organic material oxidization affects
 453 planktonic foraminifera shells co-deposited with such aggregates, but, it does not significantly
 454 affect the seafloor surface or outside of the aggregates (i.e., the habitat area of benthic
 455 foraminifera). These findings suggests that the planktonic foraminiferal CTDX is not a suitable
 456 proxy at sites with high organic material deposition like upwelling system. The benthic
 457 foraminiferal B/Ca ratio is rather appropriate for use in such sample sites.

458
459

460 **4.2. Deep seawater $[\text{CO}_3^{2-}]$ proxies: The characteristics of CTDX and B/Ca proxy**

461 In this study, the characteristics of CTDX proxy were determined by measuring the
 462 dissolution intensity of four species of planktic foraminifera and comparing the several
 463 parameters derived from seafloor sediment samples in the South Atlantic. First, the results of
 464 inter-species comparisons (Figure 5) showed that the CTDX varies among the species,
 465 suggesting that species-specific application is required for accurate reconstruction. Nevertheless,
 466 our results suggested that the CTDX of all species are applicable as shell dissolution proxy. This

467 indicates that multiple species of planktonic foraminifera are applicable as deep-water $[CO_3^{2-}]$
 468 proxy by establishing proxy calibration for each species. This is one of the essential advantages
 469 of using CTDX over conventional proxies based on the B/Ca ratio of benthic foraminifera.
 470 Therefore, it enables us to apply this new proxy to the foraminifera poor sediment cores, where it
 471 is challenging to collect single species continuously. It also allows us to compare the
 472 reconstructed data between sites from different locations with different planktic locations
 473 foraminiferal species compositions.

474 Second, the relationship between the CTDX and the deep seawater $\Delta[CO_3^{2-}]$ suggested
 475 that the CTDX significantly correlated with deep seawater $\Delta[CO_3^{2-}]$ only under the low deep
 476 seawater $\Delta[CO_3^{2-}]$ condition ($< 10 \mu\text{mol kg}^{-1}$) (Figure 6, and Figure 9). However, under the
 477 high deep seawater $\Delta[CO_3^{2-}]$ condition ($> 10 \mu\text{mol kg}^{-1}$), the values of planktic
 478 foraminiferal CTDX were almost constant. Similar results were also represented by the
 479 comparison between shell dissolution proxy and deep seawater $\Delta[CO_3^{2-}]$, suggesting the
 480 saturation of shell dissolution proxy at the sites of high deep seawater $\Delta[CO_3^{2-}]$ (> 10
 481 $\mu\text{mol/kg}$) [Johnstone et al., 2010]. Furthermore, under the extremely low deep seawater
 482 $\Delta[CO_3^{2-}]$ condition ($< -20 \mu\text{mol kg}^{-1}$), the CTDX seems to saturate around the values of 60
 483 (Figure 9). This implies that planktonic foraminiferal shells which appear intact (i.e., which
 484 are not broken or fragmented and retain the outermost chamber) show maximum CTDX
 485 values of around 60. It is likely that with further progressing dissolution the shells lose
 486 structural integrity, break into fragments and would fall outside of the sample selection for
 487 CT scanning. From the above, we conclude that the CTDX proxy works effectively under
 488 deep seawater $\Delta[CO_3^{2-}]$ lower than $10 \mu\text{mol kg}^{-1}$ and higher than $-20 \mu\text{mol kg}^{-1}$.
 489 Alternatively, we suppose that the analysis of fragmented individual is useful for applying
 490 CTDX under the significantly low deep seawater $\Delta[CO_3^{2-}]$ condition ($< -20 \mu\text{mol kg}^{-1}$).

491 We also evaluated the accuracy of the deep seawater $[CO_3^{2-}]$ reconstruction by each
 492 proxy. Under the low deep seawater $\Delta[CO_3^{2-}]$ ($< 10 \mu\text{mol/kg}$) condition, the proxy of CTDX
 493 showed a correlation with the deep seawater $\Delta[CO_3^{2-}]$ and the conventional proxy of benthic
 494 foraminiferal B/Ca ratio (Figure 7). These results support our interpretation that the proxy of
 495 CTDX can serve as an indicator of deep seawater $\Delta[CO_3^{2-}]$. Nevertheless, comparing these two
 496 proxies, we found two peculiar sites (Sites GeoB-1715 and 1729) where the CTDX and B/Ca
 497 ratio values deviate (Figure 8). The sediment samples at these two sites are rich in carbonate ($>$
 498 80%), and the proxy of CTDX shows the occurrence of carbonate dissolution and relatively high
 499 values of benthic foraminiferal B/Ca ratio than general estimation. We speculate that the process
 500 of carbonate compensation in surface sediment may have raised $[CO_3^{2-}]$ in the porewater and
 501 contributed to the higher values of the benthic foraminiferal B/Ca ratio in a way similar to the
 502 speculated protective effect of aragonite dissolution on carbonate preservation described by
 503 Sulpice et al. (2022). To evaluate this speculation, we investigated the difference in total
 504 alkalinity of porewater in the sediment surface (upper 5 cm) and the overlying bottom water
 505 (Hensen et al., 2003a-d). The total alkalinity is a valuable indicator that relates to the seawater
 506 $[CO_3^{2-}]$ and is controlled by the carbonate dissolution in the sediment, which enables us to
 507 presume the geochemical process in the sediment surface. The profiles of chemical parameters at
 508 Site GeoB-1715 and 1729 showed that the total alkalinity in the pore water (average of the upper
 509 5 cm) is more than $200 \mu\text{mol kg}^{-1}$ higher than in overlying bottom water as follows: GeoB-1715
 510 (bottom water: $2354 \mu\text{mol kg}^{-1}$, porewater average: $2583 \mu\text{mol kg}^{-1}$) and GeoB-1729 (bottom
 511 water: $2359 \mu\text{mol kg}^{-1}$, porewater average: $2653 \mu\text{mol kg}^{-1}$). In contrast, at Site GeoB-3804 and
 512 3827 with appropriate benthic foraminiferal B/Ca ratio for the general estimation, the difference

513 in the total alkalinity between pore water and overlying bottom water is relatively small as
 514 follows: GeoB-3804 (bottom water: $2348 \mu\text{mol kg}^{-1}$, porewater average: $2458 \mu\text{mol kg}^{-1}$) and
 515 GeoB-3827 (bottom water: $2342 \mu\text{mol kg}^{-1}$, porewater average: $2275 \mu\text{mol kg}^{-1}$). These results
 516 imply that carbonate dissolution at the sediment surface discharges carbonate ions and raises the
 517 porewater's total alkalinity, altering the calcification condition for benthic foraminifera. From the
 518 above, we consider that the strong carbonate dissolution in the carbonate-rich sediment is one of
 519 the principles controlling factors of the benthic foraminiferal B/Ca ratio.
 520

521 5 Conclusions

522 The assessments in planktic foraminiferal shell dissolution intensity, represented by
 523 CTDX, were directly compared with the data of B/Ca in benthic foraminifera in the same sample
 524 and the other proxies of conditions at each site (deep-water $\Delta[\text{CO}_3^{2-}]$, sedimentation rate, and
 525 Organic carbon accumulation rate). In addition, inter-species variation in CTDX of four species
 526 of planktic foraminifera were assessed. Our results proved that CTDX of each planktic
 527 foraminifera is generally controlled by deep-water $\Delta[\text{CO}_3^{2-}]$ variation like a conventional proxy
 528 of benthic foraminiferal B/Ca ratio. We suggested that four species (*G. bulloides*, *G. inflata*, *G.*
 529 *ruber*, and *T. sacculifer*) of planktonic foraminiferal CTDX are applicable as a quantitative proxy
 530 for carbonate dissolution intensity, while we recommend species-specific use of CTDX for
 531 accurate reconstruction because there is slight difference in sensitivity to dissolution. On the
 532 other hand, the effect of variation in sedimentation rate is not a significant factor in carbonate
 533 dissolution in the sediment surface if the difference in sedimentation rate is 5-to-10-fold
 534 difference or less. Based on the above results, we concluded that the proxy of planktic
 535 foraminiferal CTDX is applicable as a quantitative deep-water $[\text{CO}_3^{2-}]$ proxy as well as a
 536 conventional proxy of benthic foraminiferal B/Ca ratio. Nevertheless, there are several caveats in
 537 the application of each proxy. First, the proxy of CTDX is useful under the specific condition of
 538 deep-water $\Delta[\text{CO}_3^{2-}]$ between -20 to $10 \mu\text{mol kg}^{-1}$, suggesting that the CTDX has a detection
 539 limit range of deep-water $[\text{CO}_3^{2-}]$. Therefore, we should exclude the seafloor sediment sample
 540 obtained from high deep-water $\Delta[\text{CO}_3^{2-}]$ condition ($> 10 \mu\text{mol kg}^{-1}$) in the process of
 541 establishing the calibration equation, and we have to note that this proxy is not reliable for
 542 reconstructing the higher deep-water $\Delta[\text{CO}_3^{2-}]$ in the application of CTDX into sediment core
 543 samples. Second, we also observed the excessive dissolution of planktic foraminifera in the
 544 supersaturated condition for calcite, which seems to be caused by the intensive input of organic
 545 material into seafloor sediment. Therefore, we consider that we should refrain from applying the
 546 CTDX proxy to the sediment sample located in the upwelling system where organic material
 547 input from the sea surface is exceptionally high. Third, we revealed that carbonate compensation,
 548 which occurs in carbonate-rich and carbonate dissolution affected sediment samples, may alter
 549 the benthic foraminiferal B/Ca ratio higher during their calcification, which may contribute to
 550 uncertainty of deep-water $[\text{CO}_3^{2-}]$ reconstruction by benthic foraminiferal B/Ca ratio.

551 Based on the suggested characteristics of CTDX, we provided the calibration formula
 552 between three species planktic foraminiferal (*G. bulloides*, *G. ruber* and *T. sacculifer*) CTDX
 553 and deep seawater $\Delta[\text{CO}_3^{2-}]$ using a number ($N = 22$) of seafloor sediment samples. Although
 554 the number of sediment samples and the distribution range of samples are inferior to the
 555 conventional proxy of benthic foraminiferal B/Ca ratio, our calibration showed that the proxy of
 556 CTDX works as well as the B/Ca proxy for deep seawater $[\text{CO}_3^{2-}]$ reconstruction under the
 557 suitable conditions. This proxy may help to fill the blank of paleo-deep-water $[\text{CO}_3^{2-}]$ data, in

558 particular, in the mid-high latitude of the North Pacific, where benthic foraminiferal B/Ca ratio
559 data are insufficient.

560

561

562 **Acknowledgments**

563 This study used samples that were collected during cruises M12/1, M20/2 and M34/3 by R/V
564 METEOR. The data reported in this paper are available in Supplemental Information. This study
565 was technically and financially supported by the Japan Agency for Marine-Earth Science and
566 Technology and the Cluster of Excellence "The Ocean Floor—Earth's Uncharted Interface"
567 funded by the German Research Foundation (DFG).

568

569

570 **Open Research**

571 The data used in this study will be available in PANGAEA (<https://www.pangaea.de/>).

572

573 **References**

574 Allen, K. A., E. L. Sikes, B. Hönisch, A. C. Elmore, T. P. Guilderson, Y. Rosenthal, and R. F.
575 Anderson (2015), Southwest Pacific deep water carbonate chemistry linked to high southern
576 latitude climate and atmospheric CO₂ during the Last Glacial Termination, *Quat. Sci. Rev.*, 122,
577 180–191. doi:10.1016/j.quascirev.2015.05.007.

578

579 Allen, K. A., E. L. Sikes, R. F. Anderson, and Y. Rosenthal (2020), Rapid Loss of CO₂ From the
580 South Pacific Ocean During the Last Glacial Termination, *Paleoceanogr. Paleoclimatology*,
581 35(2), 1–13. doi:10.1029/2019PA003766.

582

583 Archer, D. E. (1991), Equatorial Pacific calcite preservation cycles: production or dissolution?
584 *Paleoceanography*, 6(5), 561–571.

585

586 Barker, S., and H. Elderfield (2002), Foraminiferal calcification response to glacial-interglacial
587 changes in atmospheric CO₂., *Science*, 297, 833–836, doi:10.1126/science.1072815.

588

589 Barnola, J. M., D. Raynaud, Y. S. Korotkevicht, and C. Lorius (1987), Vostok ice core provides
590 160,000-year record of atmospheric CO₂, *Nat. Geosci.*, 329, 408.

591

592

593 Bé, A.W.H., D.A. Caron, O.R. Anderson (1981), Effects of feeding frequency on life processes
594 of the planktonic foraminifer *Globigerinoides sacculifer* in laboratory culture, *Journal of the*

- 595 *Marine Biological Association of the United Kingdom*, 61, 257–277.
- 596
- 597 Berger, W. H. (1970), Diversity of Planktonic Foraminifera in Deep-Sea Sediments, *Science* (80-
598 .), 168(3937), 1345–1347, doi:10.1126/science.168.3937.1345.
- 599
- 600 Berger, W. H., F. L. Parker, and L. Jolla (1982), Foraminifera on the deep-sea floor: lysocline
601 and dissolution rate, *Oceanol. Acta*, 5(2), 249–258.
- 602
- 603 Berger, W. (1989), Global maps of ocean productivity, in *Productivity of the Ocean: Present and*
604 *Past*, edited by W. H. Berger, V. S. Smetacek, and G. Wefer, pp. 429–455, John Wiley, New
605 York
- 606
- 607 Bleil, U. (2001), Report and preliminary results of Meteor Cruise M 46/3, Montevideo - Mar del
608 Plata, 04.01-07.02.2000., Berichte, Fachbereich Geowissenschaften, Univ. Bremen, 172.
- 609
- 610 Broecker, W. S., and E. Clark (2001), Glacial-to-Holocene redistribution of carbonate ion in the
611 deep sea., *Science*, 294, 2152–2155, doi:10.1126/science.1064171.
- 612
- 613 Brown, R. E., L. D. Anderson, E. Thomas, and J. C. Zachos (2011), A core-top calibration of
614 B/Ca in the benthic foraminifers Nuttallides umbonifera and Oridorsalis umbonatus: A proxy for
615 Cenozoic bottom water carbonate saturation, *Earth Planet. Sci. Lett.*, 310(3–4), 360–368.
616 doi:10.1016/j.epsl.2011.08.023.
- 617
- 618 Brown, S. J., and H. Elderfield (1996), Variations in Mg/Ca and Sr/Ca ratios of planktonic
619 foraminifera caused by postdepositional dissolution: Evidence of shallow Mg-dependent
620 dissolution, , 11(5), 543–551.
- 621
- 622 Emerson, S. and M. Bender (1981), Carbon fluxes at the sediment-water interface of the deep-
623 sea: calcium carbonate preservation, *Journal of Marine Research*, 39, 139–162, 1981.
- 624
- 625 Geslin, E., P. Heinz, F. Jorissen, and C. Hemleben (2004), Migratory responses of deep-sea
626 benthic foraminifera to variable oxygen conditions: Laboratory investigations, *Mar. Micropaleontol.*, 53(3–4), 227–243, doi:10.1016/j.marmicro.2004.05.010.
- 628
- 629 Gooday, A. J. (2003), Benthic foraminifera (protista) as tools in deep-water palaeoceanography:
630 Environmental influences on faunal characteristics, *Adv. Mar. Biol.*, 46, 1–90.
- 631
- 632 Hales, B. (2003), Respiration, dissolution, and the lysocline, *Paleoceanography*, 18(4), 1–14,
633 doi:10.1029/2003PA000915.
- 634
- 635 Hales, B., and S. Emerson (1996), Calcite dissolution in sediments of the Ontong-Java Plateau:
636 In situ measurements of pore water O₂ and pH, *Global Biogeochem. Cycles*, 10(3), 527–541.
- 637
- 638 Hensen, Christian; Zabel, Matthias (2003a): Geochemistry of porewater in sediment core
639 GeoB1715-3. PANGAEA, <https://doi.org/10.1594/PANGAEA.105409>
- 640

- 641 Hensen, Christian; Zabel, Matthias (2003b): Geochemistry of porewater in sediment core
642 GeoB1729-2. PANGAEA, <https://doi.org/10.1594/PANGAEA.105421>
- 643 Hensen, Christian; Kasten, Sabine (2003c): Geochemistry of porewater in sediment core
644 GeoB3804-2. PANGAEA, <https://doi.org/10.1594/PANGAEA.105848>
- 645
- 646 Hensen, Christian; Kasten, Sabine (2003d): Geochemistry of porewater in sediment core
647 GeoB3827-1. PANGAEA, <https://doi.org/10.1594/PANGAEA.105893>
- 648
- 649 Hemming, N. G., and G. N. Hanson (1992), Boron isotopic composition and concentration in
650 modern marine carbonates, *Geochim. Cosmochim. Acta*, 56(1), 537–543.
651 [https://doi:10.1016/0016-7037\(92\)90151-8](https://doi:10.1016/0016-7037(92)90151-8).
- 652
- 653 Iwasaki, S., K. Kimoto, O. Sasaki, H. Kano, M. C. Honda, and Y. Okazaki (2015), Observation
654 of the dissolution process of Globigerina bulloides tests (planktic foraminifera) by X-ray
655 microcomputed tomography, *Paleoceanography*, 30(4), 317–331, doi:10.1002/2014PA002639.
- 656
- 657 Iwasaki, S., K. Kimoto, O. Sasaki, H. Kano, and H. Uchida (2019), Sensitivity of planktic
658 foraminiferal test bulk density to ocean acidification, *Sci. Rep.*, 9, 1–9, doi:10.1038/s41598-019-
659 46041-x.
- 660
- 661 Iwasaki, S., L. Lembke-jene, K. Nagashima, H. W. Arz, N. Harada, K. Kimoto, and F. Lamy
662 (2022), Evidence for late-glacial oceanic carbon redistribution and discharge from the Pacific
663 Southern Ocean, *Nat. Commun.*, 13(6250), doi:10.1038/s41467-022-33753-4.
- 664
- 665 Jahnke, R. A., D. B. Craven, and J.-F. Gaillard (1994), The influence of organic matter
666 diagenesis on CaCO₃ dissolution at the deep-sea floor, *Geochim. Cosmochim. Acta*, 58(13),
667 2799–2809.
- 668
- 669 Johnstone, H. J. H., M. Schulz, S. Barker, and H. Elderfield (2010), Inside story: An X-ray
670 computed tomography method for assessing dissolution in the tests of planktonic foraminifera,
671 *Mar. Micropaleontol.*, 77(1–2), 58–70, doi:10.1016/j.marmicro.2010.07.004.
- 672
- 673 Key, R. M., A. Kozyr, C. L. Sabine, K. Lee, R. Wanninkhof, J. L. Bullister, R. A. Feely, F. J.
674 Millero, C. Mordy, and T. H. Peng (2004), A global ocean carbon climatology: Results from
675 Global Data Analysis Project (GLODAP), *Global Biogeochem. Cycles*, 18, 1–23,
676 doi:10.1029/2004GB002247.
- 677
- 678 Kitazato, H. et al. (2000), Seasonal phytodetritus deposition and responses of bathyal benthic
679 foraminiferal populations in Sagami Bay, Japan: Preliminary results from “Project Sagami 1996–
680 1999,” *Mar. Micropaleontol.*, 40(3), 135–149, doi:10.1016/S0377-8398(00)00036-0.
- 681
- 682 Kucera, M. (2007). Chapter Six: Planktonic foraminifera as tracers of past oceanic environments.
683 *Developments in Marine Geology*, 1, 213–262.
- 684
- 685 Lohmann, G. P. (1995), A model for variation in the chemistry of planktonic foraminifera due to
686 secondary calcification and selective dissolution, *Paleoceanography*, 10(3), 445–457.

- 687
688 Marshall, B. J., R. C. Thunell, M. J. Henehan, Y. Astor, and K. E. Wejnert (2013), Planktonic
689 foraminiferal area density as a proxy for carbonate ion concentration: A calibration study using
690 the Cariaco Basin ocean time series, *Paleoceanography*, 28(2), 363–376,
691 doi:10.1002/palo.20034.
- 692
693 Milliman, J. D. (1993), Production and accumulation of calcium carbonate in the ocean: Budget
694 of a nonsteady state, *Global Biogeochem. Cycles*, 7(4), 927–957, doi:10.1038/181669b0.
- 695
696 Mollenhauer, G et al. (2004): Organic carbon accumulation in the South Atlantic Ocean: its
697 modern, mid-Holocene and last glacial distribution. *Global and Planetary Change*, 40(3-4), 249-
698 266, <https://doi.org/10.1016/j.gloplacha.2003.08.002>
- 699 Müller, Peter J (2004): Carbon and nitrogen data of sediment core GeoB1715-1. Department of
700 Geosciences, Bremen University, PANGAEA, <https://doi.org/10.1594/PANGAEA.143542>
- 701
702 Morard, R. et al. (2019), Genetic and morphological divergence in the warm-water planktonic
703 foraminifera genus Globigerinoides, *PLoS One*, 14(12), 1–30,
704 doi:10.1371/journal.pone.0225246.
- 705
706 Peterson, L. C., and W. L. Prell (1985), Carbonate dissolution in recent sediments of the eastern
707 Equatorial Indian Ocean: preservation patterns and carbonate loss above the lysocline, *Mar. Geol.*, 64, 259–290.
- 708
709 Petit, J. R. et al. (1999), Climate and atmospheric history of the past 420,000 years from the
710 Vostok ice core, Antarctica, *Nature*, 399(6735), 429–436. <https://doi.org/10.1038/20859>.
- 711
712 Rae, J. W. B., G. L. Foster, D. N. Schmidt, and T. Elliott (2011), Boron isotopes and B/Ca in
713 benthic foraminifera: Proxies for the deep ocean carbonate system, *Earth Planet. Sci. Lett.*,
714 302(3–4), 403–413. <https://doi.org/10.1016/j.epsl.2010.12.034>.
- 715
716 Raitzsch, M., E. C. Hathorne, H. Kuhnert, J. Groeneveld, and T. Bickert (2011), Modern and late
717 pleistocene B/Ca ratios of the benthic foraminifer Planulina wuellerstorfidetermined with laser
718 ablation ICP-MS, *Geology*, 39(11), 1039–1042. doi:10.1130/G32009.1.
- 719
720 Schiebel, R. (2002), Planktic foraminiferal sedimentation and the marine calcite budget, *Global
721 Biogeochem. Cycles*, 16(4), 3-1-3–21. doi:10.1029/2001gb001459.
- 722
723
724 Schulz, HD and et al(1992)Bericht und erste Ergebnisse über die Meteor-Fahrt M20/2, Abidjan-
725 Dakar, 27.12.1991-3.2.1992.Berichte aus dem Fachbereich Geowissenschaften der Universität
726 Bremen, 025. Department of Geosciences, Bremen University. urn:nbn:de:gbv:46-ep000101614
- 727
728 Sigman, D. M., and E. A. Boyle (2000), Glacial/interglacial variations in atmospheric carbon
729 dioxide, *Nature*, 407(19), 859–869. <https://doi.org/10.1038/35038000>.
- 730
731

- 732 Sulpis, O., P. Agrawal, M. Wolthers, G. Munhoven, M. Walker, and J. J. Middelburg (2022),
 733 Aragonite dissolution protects calcite at the seafloor, *Nat. Commun.*, 13(1), 1–8,
 734 doi:10.1038/s41467-022-28711-z.
- 735
- 736 Volbers, A. N., and R. Henrich (2002), Late Quaternary variations in calcium carbonate
 737 preservation of deep-sea sediments in the northern Cape Basin: results from a multiproxy
 738 approach, *Mar. Geol.*, 180(1–4), 203–220, doi:10.1016/S0025-3227(01)00214-6.
- 739
- 740 Wefer, G and et al (1990), Bericht über die Meteor-Fahrt M12/1, Kapstadt-Funchal, 13.3.-
 741 14.4.1990. Berichte aus dem Fachbereich Geowissenschaften der Universität Bremen, 011.
 742 Department of Geosciences, Bremen University. urn:nbn:de:gbv:46-ep000101534
- 743
- 744 Wefer, G. (1996), Report and preliminary results of METEOR-Cruise M34/3, Walvis Bay -
 745 Recife, 21.2.-17.3.1996., Berichte, Fachbereich Geowissenschaften, Univ. Bremen, 79.
- 746
- 747 Yu, J., and H. Elderfield (2007), Benthic foraminiferal B/Ca ratios reflect deep water carbonate
 748 saturation state, *Earth Planet. Sci. Lett.*, 258(1–2), 73–86. https://doi:10.1016/j.epsl.2007.03.025.
- 749
- 750 Yu, J., R. F. Anderson, Z. Jin, J. W. B. Rae, B. N. Opdyke, and S. M. Eggins (2013), Responses
 751 of the deep ocean carbonate system to carbon reorganization during the Last Glacial-interglacial
 752 cycle, *Quat. Sci. Rev.*, 76, 39–52. doi:10.1016/j.quascirev.2013.06.020.
- 753
- 754 Yu, J. et al. (2016), Sequestration of carbon in the deep Atlantic during the last glaciation, *Nat.*
755 Geosci., 9(4), 319–324. doi:10.1038/ngeo2657.
- 756
- 757 Yu, J. et al. (2020), Last glacial atmospheric CO₂ decline due to widespread Pacific deep-water
 758 expansion, *Nat. Geosci.*, 13, 628–633, doi:10.1038/s41561-020-0610-5.
- 759
- 760

761 Figure chaptions

762 **Figure 1.** The locations of multiple corer samples in the South Atlantic used in this study. The
 763 section along the yellow line is showing the spatial distribution of the degree of carbonate
 764 saturation ($\Delta[\text{CO}_3^{2-}]$) in the study area.

765

766 **Figure 2.** B/Ca ratio in shells of the benthic foraminifera *Cibicidoides wuellerstorfi* in core top
 767 samples plotted against deep-water $\Delta[\text{CO}_3^{2-}]$. The data of B/Ca ratio of benthic foraminifera in
 768 the core-top sample used in this study are shown by blue squares. Data are derived from [Rae et al. \(2011\)](#), [Raitzsch et al. \(2011\)](#), and [Yu and Elderfield \(2007\)](#).

770

771 **Figure 3.** Protocol to calculate the foraminiferal shell dissolution index (CTDX) start from raw
 772 sequential X-ray image data (a). (b) Contaminants in the shell sample are removed by manual
 773 deleting. (c) Apply threshold to distinguish between calcite material and surrounding
 774 environment. Extract CT number histogram from cleaned and threshold 3D data. (d) Scaling X
 775 and Y-axes of CT number histogram. (e) Calculation of CTDX (%).

776

777 **Figure 4.** Changes in cross-sectional isosurface images and CT number histograms of four major
 778 species of planktonic foraminiferal shells (*G. bulloides*, *G. inflata*, *G. ruber* and *T. sacculifer*)
 779 with the progression of dissolution. Shells were obtained from three core top samples (GeoB-
 780 1728, 1729, and 3827). The condition of selected tests, which have CTDX similar to average of
 781 each sample set, are shown. $\Delta[\text{CO}_3^{2-}]$ at the nearest GLODAP stations at the core-top sample
 782 depths ranged from -4.3 to $23.8 \mu\text{mol kg}^{-1}$. The dashed line in the CT number histograms shows
 783 the threshold (50) between low and high values.
 784

785

785 **Figure 5.** Inter species comparison of *G. bulloides* CTDX with other three species obtained from
 786 same core-top samples. The square of the correlation coefficient (R^2) and the type I error rate (p -
 787 value) are also shown.
 788

789

789 **Figure 6.** Investigation in controlling factor of foraminiferal shell dissolution intensity. (a)
 790 Bottom water $\Delta[\text{CO}_3^{2-}]$ ($\mu\text{mol kg}^{-1}$), (b) Linear Sedimentation Rate (cm kyr^{-1}), and (c) Organic
 791 carbon accumulation rate ($\text{g cm}^{-2} \text{kyr}^{-1}$) versus Planktonic foraminifera CTDX (%) at each
 792 sampling site. The data points at the sites located in the Benguela upwelling system (GeoB-1715,
 793 1720 and 1721) with high organic carbon accumulation rate are surrounded by dotted line.
 794

795

795 **Figure 7.** Relationship between planktonic foraminiferal CTDX of (a) *G. bulloides*, (b) *G.*
 796 *inflata*, (c) *G. ruber*, and (d) *T. sacculifer* and B/Ca ratio of *C. wuellerstorfi* ($\mu\text{mol mol}^{-1}$) in each
 797 core-top sample. The sampling sites located in the Benguela upwelling system with high organic
 798 carbon flux are shown by gray circle. The regression line and the square of the correlation
 799 coefficient (R^2) are also shown.
 800

801

801 **Figure 8.** Comparison of the plots of *G. bulloides* CTDX and B/Ca ratio of *C. wuellerstorfi*
 802 against bottom seawater $\Delta[\text{CO}_3^{2-}]$ under the condition of low bottom seawater $\Delta[\text{CO}_3^{2-}]$ (< 10
 803 $\mu\text{mol kg}^{-1}$). The B/Ca ratio of *C. wuellerstorfi* at the site GeoB-1715, 1729 and 3803 are
 804 relatively higher than *G. bulloides* CTDX.
 805

806

806 **Figure 9.** The CTDX of planktonic foraminifera (*G. bulloides*, *G. ruber* and *T. sacculifer*) in
 807 core top samples plotted against deep-water $\Delta[\text{CO}_3^{2-}]$. Core-top samples are obtained from this
 808 study and previous studies (Iwasaki et al., 2019 and 2022).
 809

810

810 **Table 1.** Multiple core sample locations, depth (m), Deep water degree of $\Delta[\text{CO}_3^{2-}]$ ($\mu\text{mol kg}^{-1}$),
 811 Linear Sedimentation Rate (cm kyr^{-1}), TOC (Total Organic Carbon) accumulation rate ($\text{g m}^{-2} \text{y}^{-1}$)
 812 and *Cibicidoides wuellerstorfi* B/Ca ratio ($\mu\text{mol mol}^{-1}$) at each sampling site.
 813
 814